A Vacuum Tolerant High Voltage System with a Low Noise and Low Power Cockcroft-Walton Photomultiplier Base

T. Masuda[a], E. Iwai[b,*], N. Kawasaki[a], E. J. Kim[c], T. K. Komatsubara[d], J. W. Lee[b], G. Y. Lim[d], Y. Maeda[a], D. Naito[a], H. Nanjo[a], T. Nomura[d], Y. D. Ri[b,**], N. Sasao[e], K. Sato[b], S. Seki[a], K. Shiomi[b], Y. Sugiyama[b], M. Togawa[b], H. Watanabe[d], T. Yamanaka[b]

[a] *Department of Physics, Kyoto University, Kyoto 606-8502, Japan*
[b] *Department of Physics, Osaka University, Osaka 560-0043, Japan*
[c] *Division of Science Education, Chonbuk National University, Jeonju, 561-756, Korea*
[d] *High Energy Accelerator Research Organization (KEK), Ibaraki 305-0801, Japan*
[e] *Research Core for Extreme Quantum World, Okayama University, Tsushima-naka 3-1-1 Kita-ku, Okayama 700-8530, Japan*

Abstract

We developed a high voltage system for the electromagnetic calorimeter of the KOTO detector. The system is designed around a low noise, low power Cockcroft-Walton (CW) photomultiplier tube base with a high gain preamplifier. The low power makes it suitable for operations in vacuum. The low noise and high gain allow detecting signals in the 1 MeV range. We achieved a final noise level below 180 μV_{rms} for a preamplifier gain of more than 40. A vacuum tolerant control system for the CW bases power distribution was also designed. This system is able to control and monitor the high voltage of each individual base.

Keywords: J-PARC, KOTO, Calorimeter, CW base, photomultiplier tube

1. Introduction

The KOTO experiment[1], located at J-PARC[2], searches for the direct CP violating $K_L \to \pi^0\nu\bar{\nu}$ decay. This decay is a flavor-changing neutral current process, and occurs via loop diagrams[3]. The presence of loops enables contributions from new physics beyond the Standard Model (SM). The branching fraction predicted by the SM is highly suppressed, and is $2.43(39)(6)\times10^{-11}$[3]. The small branching fraction, together with the precision of the SM prediction, make this decay very sensitive to possible effects from new physics.

Figure 1 shows a cross-sectional view of the KOTO detector. The detector consists of two parts: a Cesium Iodide (CsI) electromagnetic calorimeter, and a group of veto counters. The calorimeter is used to identify the $K_L \to \pi^0\nu\bar{\nu}$ decay by measuring the energies and positions of the two photons from the π^0 while the veto counters ensure that there is no extra particle in the decay. The calorimeter and most of the veto counters are located inside a vacuum chamber in order to minimize the material in front of the detectors. The area around the detectors is evacuated to the level of 1 Pa.

We use photomultiplier tubes (PMTs) for readout of the calorimeter. They require high voltage (HV) power supplies able to operate in vacuum. We adopted a Cockcroft-Walton (CW) base as a solution. CW bases have been used extensively in particle physics experiments[4–7]. They contain a high voltage generating circuit[8] which consists of an oscillator and a ladder of diodes and capacitors. Each step of the ladder provides voltage to a dynode. There are advantages and disadvantages in using a CW base. The most attractive feature is the lack of bleeder current, which results in low power consumption. The tolerance to high counting rates is superior to that of a generic resistor divider base, since the presence of capacitors smoothes the voltage at the dynode, making it stable even when the anode current is large. In addition, a CW base can be operated with a low voltage controller. On the other hand, the internal large-voltage oscillator and switching diodes can be sources of electrical noise. Also the voltage divider ratio is limited by the number of diode and capacitor ladders, which hinders the ability to fine tune this ratio.

The two key issues that had to be confronted before the final decision to use CW bases were their ability to withstand vacuum conditions and to achieve the noise level required by the experiment. This resulted in the design of a preamplifier using several noise reduction and discharge protection techniques. It also spurred the development of a HV control system with low power consumption and an ability to operate in vacuum.

The remaining of this paper is organized as following: Section 2 describes the KOTO CsI calorimeter; Section 3 is dedicated to the description of the HV system designed

*Present Address : High Energy Accelerator Research Organization (KEK).
**Present Address : Hitachi Advanced Digital, Inc., Japan.
Email address: taka@scphys.kyoto-u.ac.jp (T. Masuda)

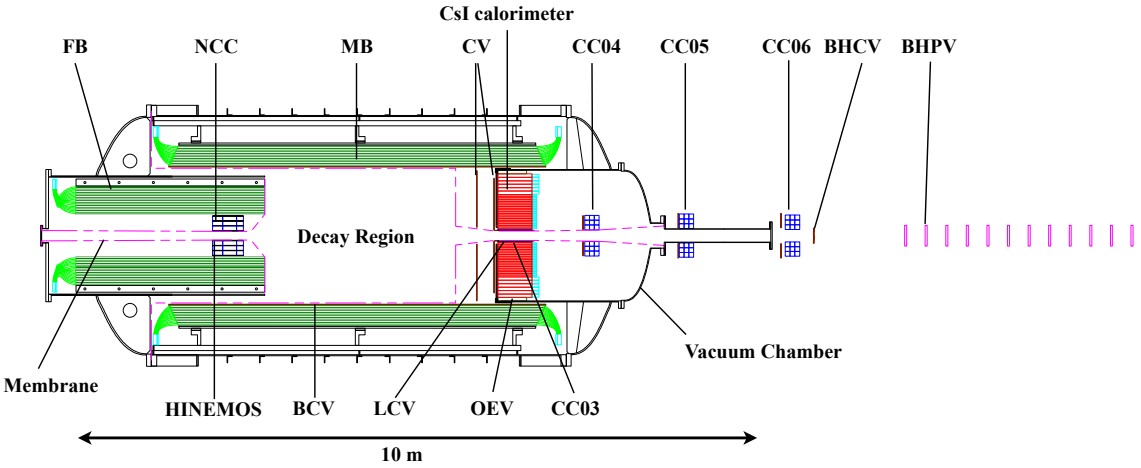

Figure 1: Cross-sectional view of the KOTO detector. The K_L beam comes in from the left hand side. HINEMOS, BCV, CV, LCV, and BHCV are charged particle veto counters made of plastic scintillators. FB, MB, and OEV are photon veto counters made of plastic scintillator interspersed with lead layers. NCC, CC03, CC04, CC05, and CC06 are photon veto counters made of CsI crystals. The BHPV acts as a veto for photons passing through the beam hole. Most of the veto counters, as well as the CsI calorimeter, are located inside a vacuum chamber. The empty region in the center is called the decay region. Membranes, shown as dashed lines, separate the detector active region, kept at 1 Pa, from the decay region, evacuated to 10^{-5} Pa.

for such calorimeter; finally, results of system performance tests are reported in Section 4.

2. CsI Calorimeter

The CsI calorimeter consists of 2716 undoped CsI crystals, stacked in a cylindrical shape of 2 m diameter and 500 mm depth along the beam direction. We use crystals of two sizes in cross section: small (25 mm × 25 mm) and large (50 mm × 50 mm). They are read out by two models of Hamamatsu PMTs: R5364 for small crystals and R5330 for large crystals. Both the CsI crystals and the PMTs were previously used in the KTeV experiment[9].

Simulation studies[10] using the Geant4 platform[11, 12] resulted in the following parameters for the readout of individual calorimeter channel. A 1 GeV upper limit for the energy dynamic range was determined by considering the expected energy deposit distribution of the $K_L \to \pi^0\nu\bar{\nu}$ decays in individual crystals. A 1 MeV lower limit was dictated by the role of the calorimeter as a veto counter. Non-linearities in the energy response affect the precision of π^0 reconstruction, and required to be below the 5% level in order to prevent background events from being mis-identified as signals. Finally, high rate tolerance was required because the counting rate of single channels near the beam was estimated around 100 kHz for a 1 MeV threshold.

3. High Voltage System

This section describes the components of the HV system: the CW base, the preamplifier, and the HV control system. Before going into the details, the requirements for their use with the CsI calorimeter are briefly summarized.

The first requirement for the HV system is low power consumption since the PMTs are located in vacuum and heat dissipation is a concern. To mitigate this problem, we adopted a CW base which has the advantage of low power consumption.

The second requirement is high amplification while keeping the noise low. The PMTs recycled from the KTeV experiment, whose characteristics are summarized in Table 1 and Table 2, have relatively low gains. In addition, the energy range for the KOTO experiment is lower than that for the KTeV experiment, because the average momentum of the K_L beam for the KOTO experiment is only 2 GeV/c while for the KTeV experiment it was 70 GeV/c. Preamplifiers able to detect signal at the 1 MeV level over the noise were specifically designed and added to the PMT outputs.

Finally a HV control system able to set the high voltage for each individual PMT was required. In order to minimize the number of cables going through the walls of the vacuum chamber, we developed a system that can operate in vacuum.

3.1. CW Base

We developed a CW base in cooperation with Matsusada Precision Inc.[13] with the requirements of low noise, low heat load, and operability in vacuum. A picture of the two types of CW bases developed for the small and large CsI crystals is shown in Figure 2. The aluminum rectangular boxes house the CW circuit while the cylindrical sections contain the PMT socket and a built-in preamplifier described in Section 3.2. These two parts are connected

Table 1: Photomultiplier tubes specifications.

item	R5330	R5364
Quantity	476	2240
Photocathode Size	34 mm dia.	15 mm dia.
Photocathode Material	Bialkali	
Window Material	Quartz	
Spectral Response	185-650 nm	
Number of Dynodes	6	5
Typical Gain	See table 2	

Table 2: PMT gain for a supply voltage of -1500 V. The voltage divider ratios are from cathode to anode.

PMT Model	Voltage Divider Ratio	PMT Gain
R5330	2:1:2:2:2:2:1	2×10^4
R5364	3:2:2:2:2:1	8×10^3

via a shielded flat-cable. The CW base specifications are listed in Table 3

The schematics of the KOTO CW base circuit are shown in Figure 3. As typical of any CW base, it contains an oscillator with a large voltage swing (150 kHz square oscillator with 100 V_{p-p}). To reduce the electrical noise induced by such a component, the aluminum boxes enclosing the CW circuit were kept at a distance of 200 mm and 500 mm from their respective preamplifiers and PMTs. In addition, both the preamplifier and the PMT were housed in a metal electrostatic shield. RC filters were placed next to the diode capacitor ladder and inside the PMT socket to reduce the ripple at the output of the CW circuit. Figure 4 shows the residual ripple at the cathode; the amplitude is less than 50 mV_{p-p} for an operation voltage of -1500 V. This corresponds to a gain deviation of less than 0.01%, given dependence of the PMT gain (G) on the output voltage (V) : $G \propto V^{0.7\sim1.2}$. Since the anode is not directly connected to the CW circuit, no ripples can be observed at the anode. The base power consumption was measured to be 60 mW for an output voltage of -1500 V and it increases linearly with the output voltage.

Table 3: KOTO CW base specifications

Parameter	Value	Notes
MODEL No.	HPMC-1.8N-04	for R5364
	HPMC-1.8N-05	for R5330
Drive Voltage	+5 V	
Drive Current	12 mA	for -1500 V
Control Voltage	0 - +1.8 V	
Output Voltage	0 - -1800 V	
Monitor Voltage	0 - +1.8 V	0 - -1800 V
Internal Oscillator	100 V_{p-p}, 150 kHz	square-wave
Cathode Ripple	< 50 mV_{p-p}	-1800 V
Number of Ladders	12	

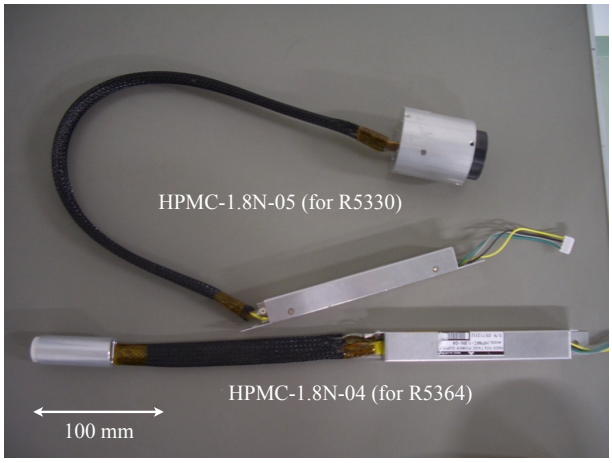

Figure 2: Picture of the two types of CW bases developed for the KOTO experiment; the electronics for the base is contained in the rectangular aluminum box, and connected via a shielded flat-cable to a cylindrical aluminum receptacle for the PMT socket and the preamplifier.

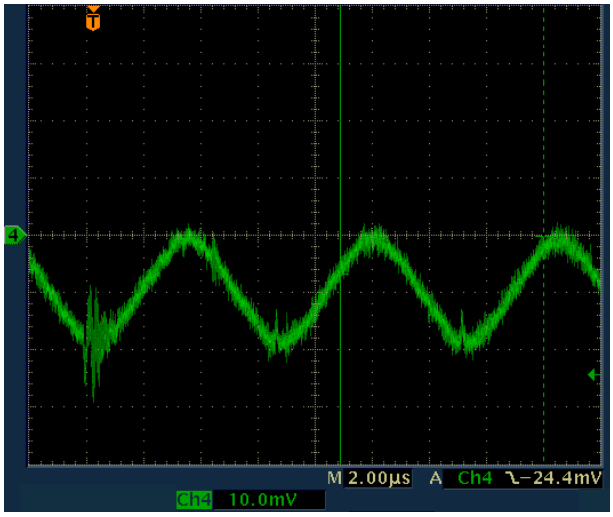

Figure 4: Scope capture of the remaining ripple at the cathode output through an AC coupling. In this measurement, the cathode was connected to ground via a 510 pF capacitor and a 1 MΩ resistor in series; the voltage drop across the resistor is shown.

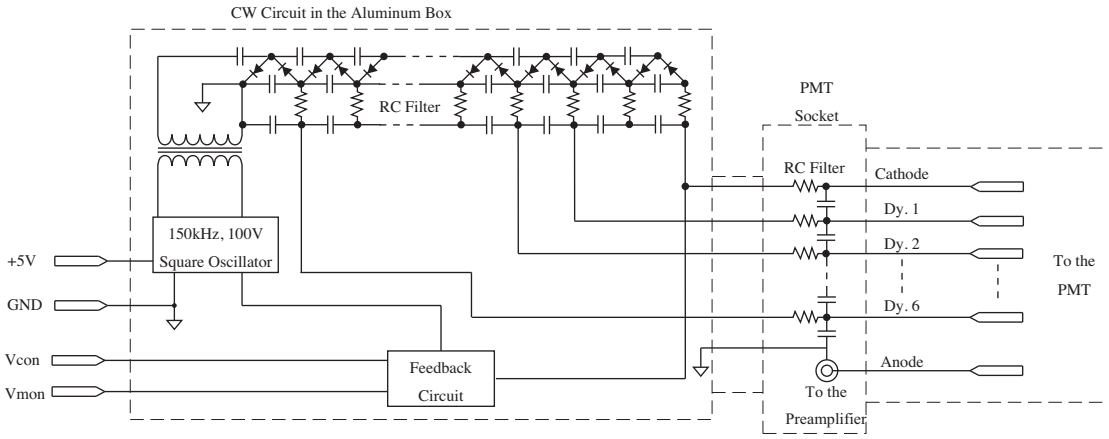

Figure 3: Circuit schematics for the HPMC-1.8N-05 base. The schematics for the HPMC-1.8N-04 base are almost the same except for the number of dynode stages and for the RC filter in the PMT socket being dropped. The dashed lines around the components represent the electric shield.

Table 4: Preamplifier specifications. The amplification values are for a 50 Ω input impedance.

Item	Value	Notes
Output	differential	
Dynamic Range	1 mV to 1 V	
Amplification	20	for R5330
	41	for R5364
	67	for low gain R5364
Noise Level	$< 180\ \mu V_{rms}$	
Decay Time	< 25 ns	faster than the 10-pole filter

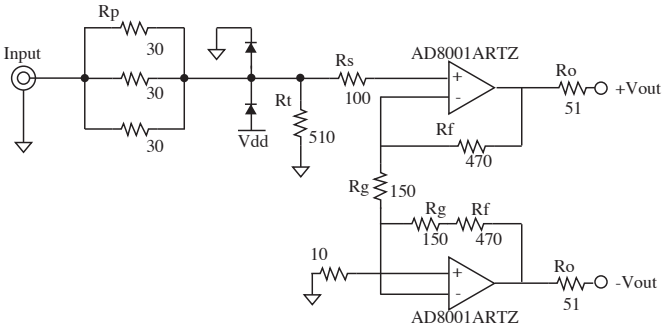

Figure 5: Schematics of the preamplifier with a gain of 41. Power supply lines are not drawn.

3.2. Preamplifier

The charge delivered by the PMT is small ($\sim 0.5\ \mu$A/MeV) and fast ($\sim$ 6 ns decay time). This signal is transferred via a 17-m-long cable and digitized at a sampling rate of 125 MHz by a 14-bit ADC module, after being shaped through a 10-pole low pass filter[14, 15]. A preamplifier with the specifications listed in Table 4 was designed to ensure the efficient propagation of the signal from the PMT to the ADC module.

Physics considerations require each channel of the CsI calorimeter to be able to detect energies between 1 MeV and 1 GeV. We decided to have a 1 V/GeV pulse height at the ADC input voltage, which corresponds to a minimum voltage detection of 1 mV over the noise. The required noise level of the preamplifier output was set to be less than 180 μV_{rms} in order to allow the detection of 1 mV signal from the noise. To accommodate for the individual variability in the PMT gain (standard deviation / mean $\sim$ 30%) and in the CsI crystals light yield ($\sim$ 20%), we used three different amplification values, as summarized in Table 4.

Figure 5 shows a schematic diagram of the preamplifier. A differential amplifier converts the single-end signal from the PMT to a differential signal. The amplification is determined by the value of the feedback resistors, R_f and R_g. The AD8001ARTZ[16] operational amplifier (op-amp) was chosen because of its low power, high speed, and high output drive characteristics. The input resistors, R_p and R_s, and the diodes between the power supply and ground rails, provide discharge protection. The resistors R_o set the output differential impedance to be 100 Ω. This circuit is mounted on a 17×22 mm^2 card, as shown in Figure 6, and connected to the PMT via a 20-mm-long coaxial cable.

The pulse amplitude and width were adjusted via the termination resistor, R_t. Assuming that the input light pulse decays exponentially, the PMT current output can be represented as:

$$I(t) = \frac{AeG}{\tau_s} \exp\left(-\frac{t}{\tau_s}\right), \quad (1)$$

where A is the light yield in units of photo-electron, e is the electron charge, G is the PMT gain, and τ_s is the decay constant of the light emission[17]. The voltage drop across R_t is

$$V(t) = -\frac{AeGR_t}{\tau - \tau_s}\left[\exp\left(-\frac{t}{\tau_s}\right) - \exp\left(-\frac{t}{\tau}\right)\right], \quad (2)$$

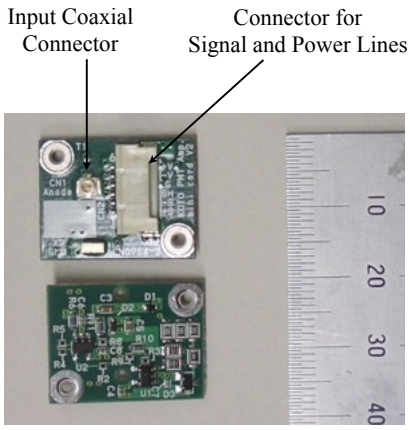

Figure 6: Photo of the front (top) and back (bottom) of the preamplifier card. The input signal is carried in via a coaxial connector mounted on the front side of the card.

$$\tau \equiv R_t C_{in}, \tag{3}$$

where C_{in} is the capacitance of the signal line, including contributions from the PMT, cable, diodes, and the op-amps. The voltage is highest at time:

$$t_0 = \frac{\tau_s \tau}{\tau_s - \tau} \ln \frac{\tau_s}{\tau}, \tag{4}$$

with a value of:

$$V(t_0) = -\frac{AeGR_t}{\tau - \tau_s} \times \left[\exp\left(-\frac{\tau \ln \frac{\tau_s}{\tau}}{\tau_s - \tau} \right) - \exp\left(-\frac{\tau_s \ln \frac{\tau_s}{\tau}}{\tau_s - \tau} \right) \right]. \tag{5}$$

Figure 7 shows the dependence of the R5364 response to light pulses from a LED on the value of the resistor R_t. The data agrees well with the prediction from Eq. 5. Increasing the value of R_t reduces the gain of the following active stage. It suppresses the noise contribution from the following stage with respect to the signal. The large value of R_t, however, increases the signal decay time τ from Eq. 3 and induces tails in the waveform after the 10-pole filter. We chose a value of R_t equal to 510 Ω. Figure 8 shows the preamplifier output together with its filtered pulse as simulated with SPICE[18] for R_t of 510 Ω.

To protect the preamplifier against electric discharge, we used three 30 Ω resistors[19] in parallel to reduce a burden on the resistors themselves, and for a redundancy. This keeps the output pulse narrow while maximizing the tolerance against discharge. The two following diodes protect the op-amp against overvoltage. The R_s resistor protects the op-amp against overcurrent. This circuitry has successfully survived discharges at voltages as high as 1750 V.

3.3. HV Control System

To adjust and monitor the high voltage of each PMT channel, we developed the HV control system shown in Figure 9. It consists of twelve controller modules connected to a PC via a commercial USB hub. Each module

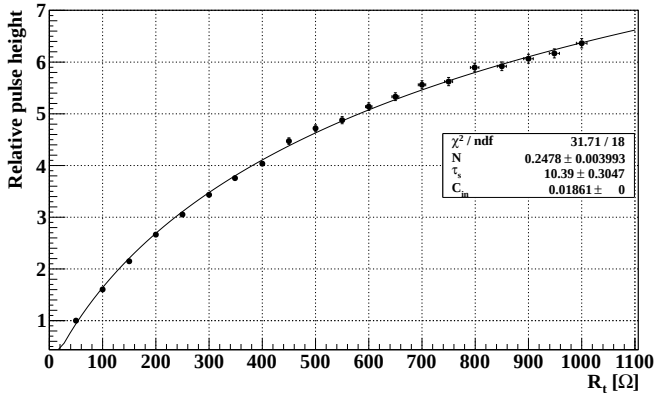

Figure 7: R_t dependence of the preamplifier pulse height in arbitrary units. Black points are measured data and the solid line is the fit using Eq. 5. N is a normalization parameter derived from setting the pulse height at 1 for R_t = 51 Ω. The C_{in} value of 0.01861 nF was obtained independently and treated as a known constant in the fit.

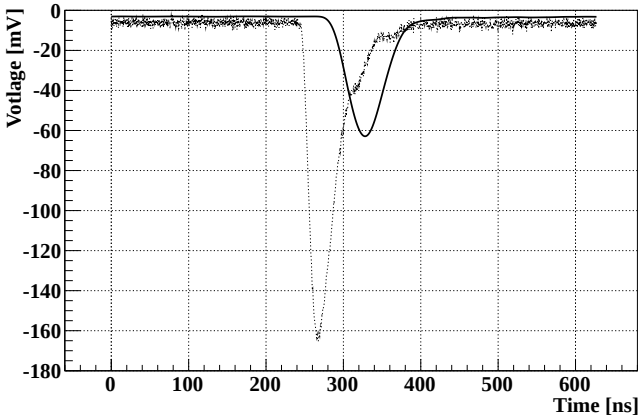

Figure 8: Preamplifier output pulse (dotted line) for a cosmic ray going through a CsI crystal overlaid to a SPICE simulation of the ADC board shaped output (solid line).

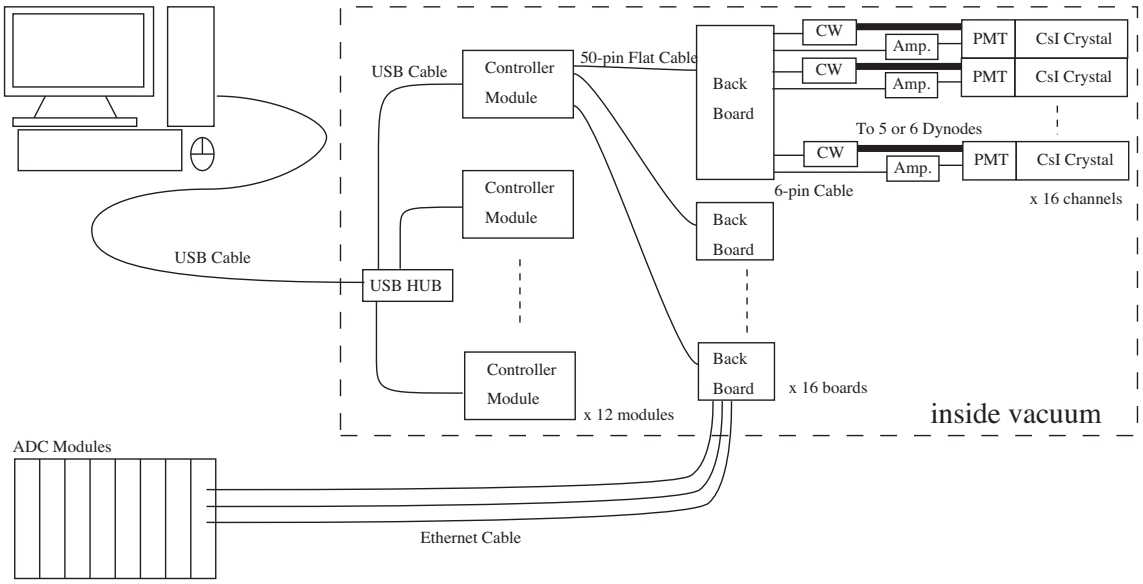

Figure 9: Overview of the HV control system. For the analog signals sent by the Back Boards to the ADC modules, we made the unconventional choice of using Ethernet cables. Although Ethernet cables are usually used to transmit digital signals, the differential analog signals are also able to be sent via Ethernet cables.

sends signals and power to sixteen custom made boards, called Back Boards, via 50-pin flat cables. Each Back Board in turn controls up to sixteen PMTs. The whole system is located inside the vacuum vessel, just behind the calorimeter.

The system was designed to power individual CW bases and preamplifiers. The high voltage of each channel can be adjusted and monitored in 1 V step. If a discharge or a malfunctioning condition is detected for a given channel, its power supply is turned off. The temperature of the Back Boards, together with the supply voltages and currents drawn by each CW base and preamplifier, are read and logged every 1 s to monitor the system stability.

3.3.1. Hardware Description

Up to sixteen CW bases are connected to a single Back Board which sends the PMT analog signal to the ADC module via a commercial Ethernet cable. A picture of the Back Board is shown in Figure 10. Sixteen Back Boards are connected to a single controller module which consists of one mother board and eight daughter boards.

The controller module uses an Atmel AVR micro-controller[20] to communicate with a PC located outside the vacuum chamber via a USB interface. Serial Peripheral Interface (SPI) and Inter-Integrated Circuit (I2C) interfaces are used for the internal communication. A Digital-to-Analog Converter (DAC) on the daughter board is used to generate the individual control voltage for the CW bases while an Analog-to-Digital Converter (ADC) on the mother board is used to monitor the status of the individual channels. A schematic view of the overall system is shown in Figure 11.

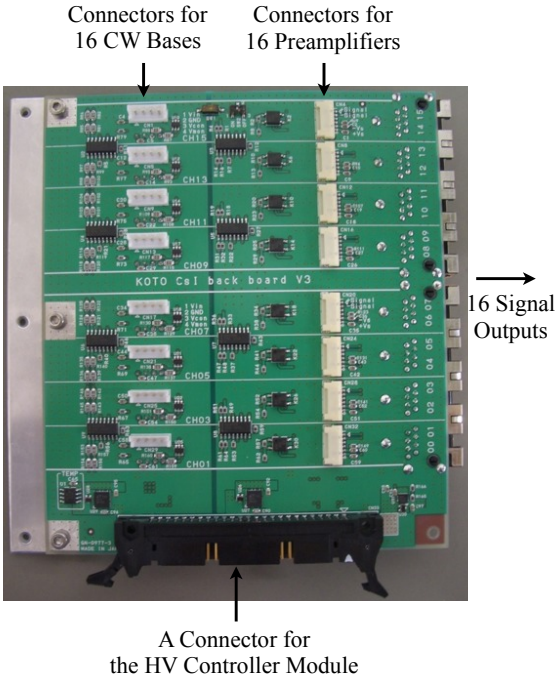

Figure 10: Back Board picture: the eight connectors on the left are for CW base power and the eight connectors on the right are for preamplifier signals and power. The same number of connectors are mounted on the other side of the board (not shown in this picture). The right-most connectors are for the Ethernet cables carrying the preamplifier output signal to the ADC module. Signals from the HV controller module arrive via the 50-pin connector at the bottom of the picture.

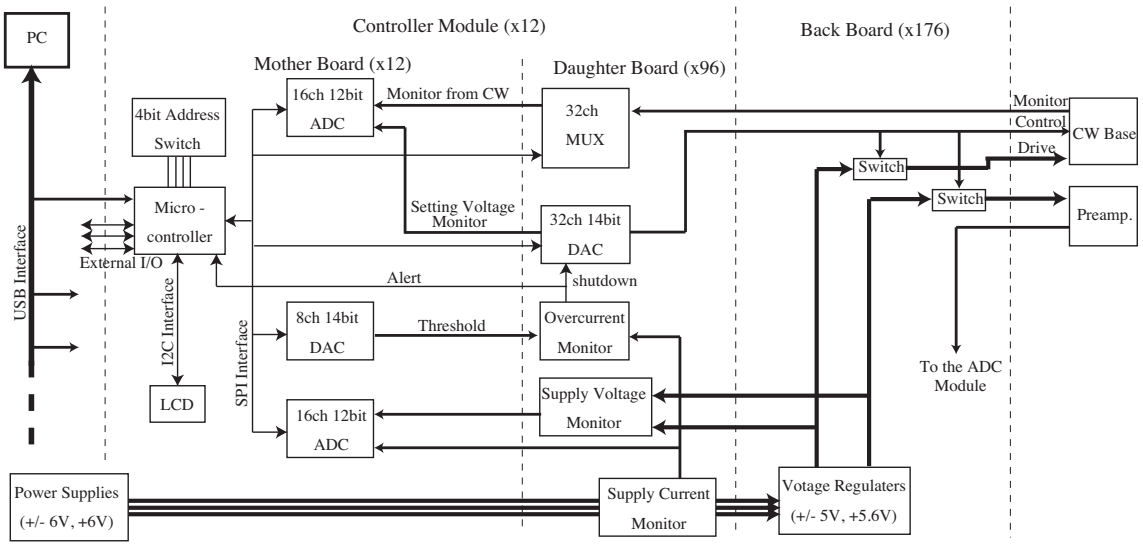

Figure 11: Schematic view of the HV control system. Thick(thin) lines indicate analog(digital) signals. The system comprises twelve controller modules. Each module is addressable via a 4-bit address switch. A Liquid-Crystal Display (LCD) is used for debug purposes. Switches mounted on the Back Board are used to turn off power to individual CW bases and preamplifiers.

3.3.2. Software Description

The firmware of the controller module instantiates a Human Interface Device (HID) class to communicate with the PC. The HID class is part of the USB specification for computer peripherals and supported by almost all operating systems. The software running on the PC is based on a Graphical User Interface (GUI) written using a Python Tkinter script. Figure 12 shows a screen shot of the GUI. The supply voltage of each channel can be controlled by clicking the map on the screen. Current and past value of numerous monitoring parameters can also be accessed this way.

4. System Performance

The performance of individual PMTs, CW bases, and preamplifiers was evaluated on a test-bench. In this section, results from these tests are reported for the individual channel noise, linearity, rate capability, and operation in vacuum. The performance of the system in situ, after its integration with the CsI calorimeter and DAQ readout, is also discussed.

4.1. Noise

In order to certify the CW bases, we measured the noise level of all bases at the output of the preamplifiers. In this measurement, the differential signals from the preamplifier were converted to single-ended signals using a converter circuit consisting of two op-amps (LMH6628[21] and ADA4899-1[16]). Figure 13 shows a typical oscilloscope capture for such measurements. Figure 14 compares the noise level distributions when the CW bases are turned off and when they output a voltage of -1500 V. The three peaks correspond to the three values of preamplifier gain.

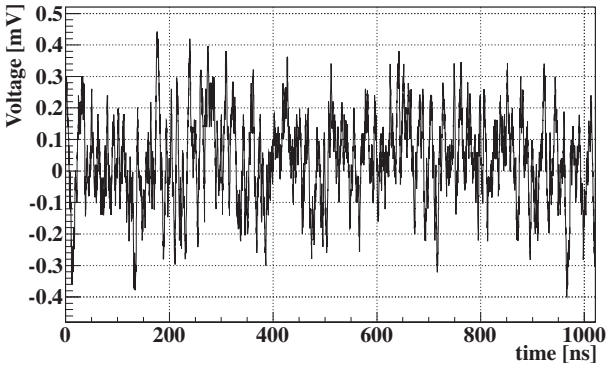

Figure 13: Typical CW base noise at the preamplifier output measured with a digital oscilloscope when the CW base is generating a voltage of -1500 V.

A few percent of the bases had noise levels above the requirement of 180 μV_{rms} if paired to the highest gain preamplifier. In that case they were used in combination with lower gain preamplifiers. This explains the cutoff at 180 μV_{rms} in Figure 14.

4.2. Linearity

We checked the linearity of the PMT, CW base, and preamplifier chain using an intensity adjustable light source and a PIN photo-diode as a reference. Figure 15 shows the linearity of the PMT chain response as a function of energy, after converting light source intensity to equivalent energy deposit. The non-linearity with respect to the PIN photo-diode readout are within 5% below 1 GeV but increase with the energy. We correct the non-linearity, particularly in the high energy region, using data from an independent set of measurements.

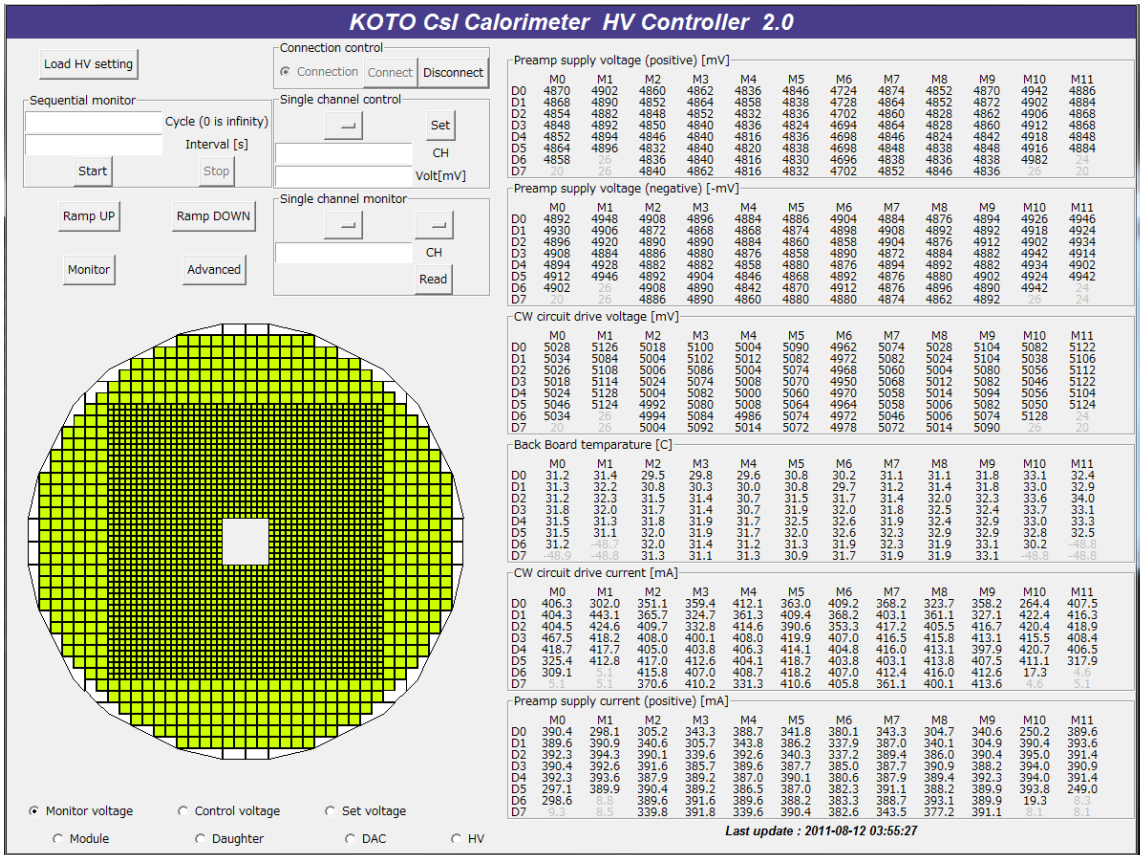

Figure 12: Screenshot of the GUI for the HV control system. The fields at the top left of the screen are for manual controlling and monitoring. The front view of the CsI calorimeter shows the operating status of each individual channel. The numbers on the right show specific monitored values and are usually refreshed every 1 s. The history of a specific value is obtained by clicking on that number.

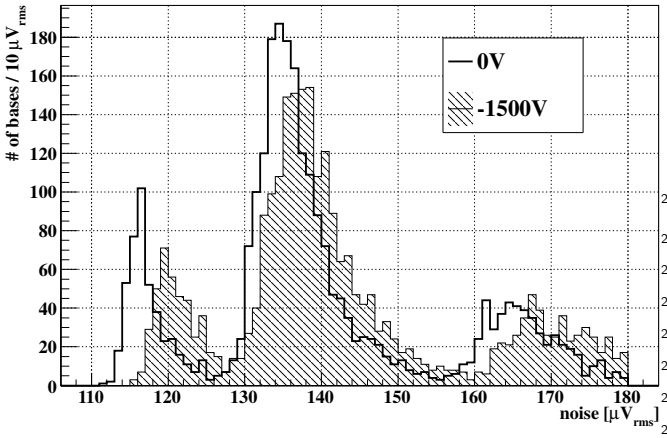

Figure 14: Distributions of noise levels in CW bases. The bold histogram shows the noise level distribution when the CW bases are turned off, and the hatched histogram represents the same distribution when the CW base output is set to -1500V. The peaks on the left are for the R5330 PMT, the peaks in the middle are for the R5364 with a gain of 41, and the peaks on the right are for the R5364 PMT with a gain of 67.

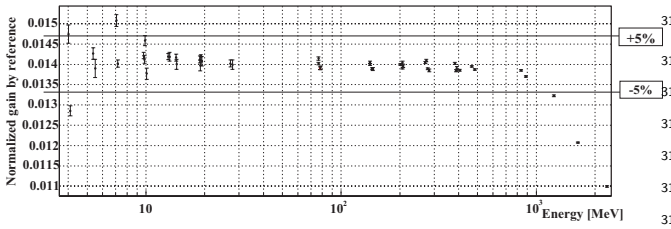

Figure 15: Linearity of output of the PMT - CW base - preamplifier chain is shown as a function of input light yield. The light yield is displayed as equivalent energy deposit. The vertical axis shows the gain normalized to the reference PIN photo diode output. The two horizontal straight lines represent the ± 5% variation from the average normalized gain distributions in the region below 500 MeV region.

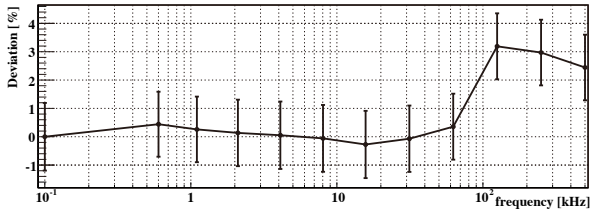

Figure 16: PMT output charge deviation, normalized to the 100 Hz value, as a function of LED pulser input rate.

4.3. Rate Capability

Using a Geant4 Monte-Carlo simulation, the single channel counting rate near the beam was estimated to be around 100 kHz for a 1 MeV threshold. The product of the hit rate times the mean energy deposit was estimated to be 2900 kHz·MeV. We checked the effect of the counting rate on the PMT output charge using a LED pulser. The light intensity was set to be 700 MeV equivalent. Figure 16 shows the results; the deviation, normalized to the 100 Hz output, was less than 1% up to 100 kHz, which is equivalent to 70000 kHz·MeV, and less than 5% up to 500 kHz.

4.4. Vacuum Tolerance

Electrical discharges are common in vacuum. The relation between pressure and discharge voltage is known as Paschen's law. To prevent the bases from discharging, we filled the aluminum rectangular box containing the CW circuit with a compound resin. Figure 17 shows the measured breakdown voltage as a function of the pressure. For typical CW bases operating of -1300 V under 1 Pa, shown as the black solid point in Figure 17, electrical discharge is not expected to be a problem.

We found that few percent of the bases discharged in vacuum[1]. After replacing them, we succeeded in operating more than 99.9% of the bases for one week in 1 Pa vacuum.

4.5. System Test

After integrating the HV system described so far in the KOTO experimental area, we tested the system performance in situ using the ADC modules for the readout of the CsI crystals signals. The following sections report the results on signal and noise characteristics, as well as on heat dissipation measurements in vacuum.

4.5.1. Signal and Noise

Figure 18 shows a pulse shape equivalent to 1 MeV recorded by the ADC at 125 MHz sampling rate. The fit function is an asymmetric gaussian of the form:

$$A \exp\left[-\frac{(t-\mu)^2}{(a(t-\mu)+\sigma)^2}\right] + C, \qquad (6)$$

[1] It was found out by the manufacturer, Matsusada Precision Inc., that the discharge can occur if structural voids are present in the compound.

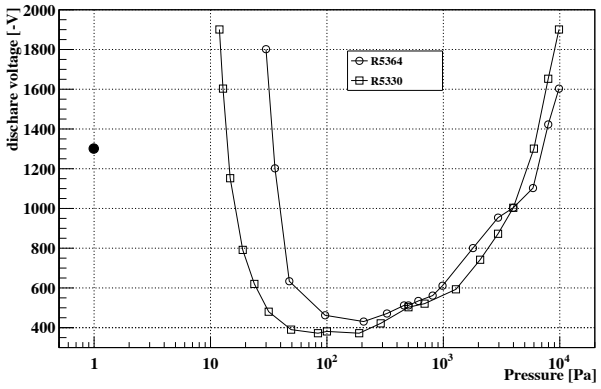

Figure 17: Discharge voltage as a function of the pressure for small and large crystal PMTs. The black solid point represents the typical CW bases operating voltage (-1300 V) and pressure inside the vacuum chamber(1 Pa). The maximum operating voltage is -1750V.

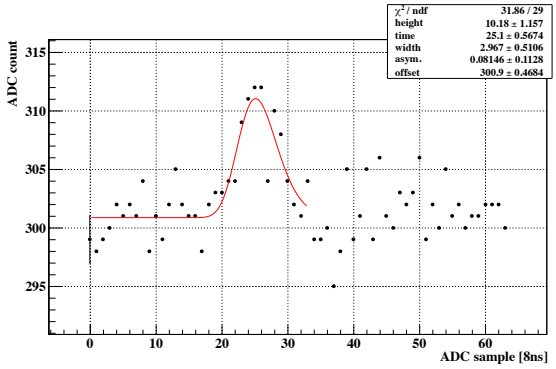

Figure 18: Typical pulse sample equivalent to 1 MeV taken by the ADC module. The vertical bar on the first point represents the noise level.

where t is the time shown along the horizontal axis, A is the pulse height, μ is the time of pulse peak, σ is the standard deviation of the gaussian distribution, a is an asymmetry parameter, and C is the vertical offset. The fit returns a pulse height of 10.2 ± 1.2 ADC counts over a noise level of ~ 2 ADC counts$_{\mathrm{rms}}$. This confirms that the system is able to resolve signals at the 1 MeV level.

Figure 19 shows the dependence of the ground noise on the preamplifier gain for a single channel. The noise is dominated by ADC intrinsic noise and has little dependence on the preamplifier gain. Figures 20 and 21 show the noise level distribution for all channels and its stability versus time. They show that the noise level was small enough and stable for a 300 hours run.

4.5.2. Heat Dissipation in Vacuum

In November 2012, we performed a test in vacuum for the full CsI calorimeter system. The heat generated by the CW base and by the preamplifier were typically 60 mW/ch

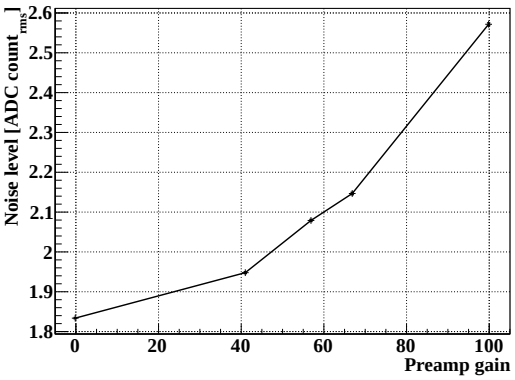

Figure 19: Ground noise dependence on the preamplifier gain for a single channel. The point at a gain of 0 represents the intrinsic noise of a typical ADC module.

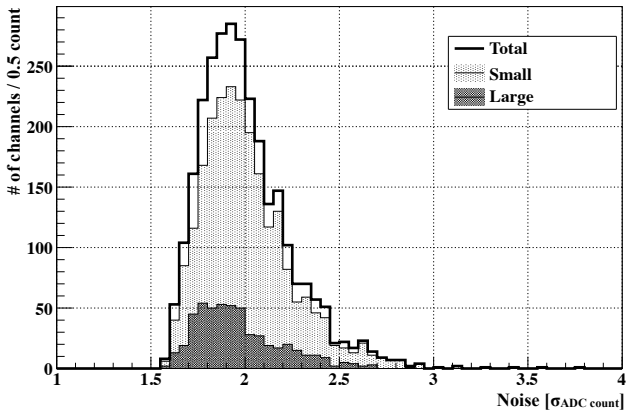

Figure 20: Ground noise distribution for all of the CsI calorimeter channels.

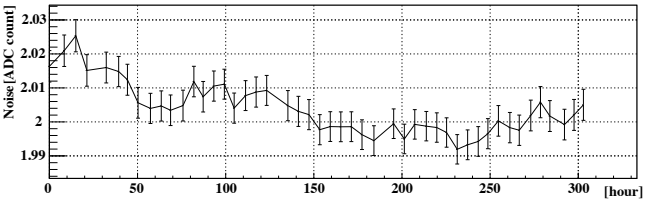

Figure 21: Time stability of the CsI calorimeter noise. Each point and relative error bar represents the mean and the standard deviation of the ground noise distribution over all the channels.

and 100 mW/ch, respectively. For the whole calorimeter, they added up to a heat load of about 440 W which was removed from the vacuum region via a water cooling system. The test lasted for 16 days in a condition of vacuum at or below 1 Pa and cooling water temperature of about 10°C. The PMT temperature ranged from 30°C to 35°C while the temperature of the CsI surface was less than 30°C. At this temperature, the loss of CsI light yield with respect to room temperature (25°C) was only 10%[2].

5. Conclusions

We developed CW bases, preamplifiers, and a HV control system that work in vacuum, and have low noise and low power consumption. A noise level below 180 μV_{rms} for a preamplifier gain of more than 40 was achieved. With this system, the KOTO CsI calorimeter can detect signals at the 1 MeV level. The system has satisfied all the design specifications and has been successfully integrated in the KOTO detector.

Acknowledgement

We would like to express our gratitude to Matsusada Precision Inc. for their continuous discussions and support on technical matters during the design and production of the CW bases. This research was supported by KEK, MEXT KAKENHI Grant Number 18071006, the Japan/US Cooperation Program, Korea NRF (2012-004554), and Taiwan NSC. Some of the authors were supported by Grant-in-Aid for JSPS Fellows from the Japan Society for the Promotion of Science.

References

[1] T. Yamanaka for the KOTO collaboration, Prog. Theor. Exp. Phys. 2012 (2012) 02B006.
[2] S. Nagamiya, Prog. Theor. Exp. Phys. 2012 (2012) 02B001.
[3] J. Brod, et al., Phys. Rev. D 83 (2011) 034030.
[4] Y. Gilitsky, et al., Nucl. Instr. and Meth. A 571 (2007) 294 – 299.
[5] B. Lu, et al., Nucl. Instr. and Meth. A 313 (1992) 135 – 141.
[6] M. Ageron, et al., Nucl. Instr. and Meth. A 656 (2011) 11 – 38.
[7] S. Nutter, et al., in: the 31th International Cosmic Ray Conference, University of Lodz, Poland, 2009.
[8] J. D. Cockcroft, E. T. S. Walton, Proc. R. Soc. London 136 (1932) 619–630.
[9] A. Alavi-Harati, et al., Phys. Rev. D 67 (2003) 012005.
[10] T. Masuda for the J-PARC E14 KOTO Collaboration, in: 2009 KAON International Conference KAON09, PoS, 2009, p. PoS(KAON09)022.
[11] S. Agostinelli, et al., Nucl. Instr. and Meth. A 506 (2003) 250 – 303.
[12] J. Allison, et al., Nuclear Science, IEEE Transactions on 53 (2006) 270–278.
[13] Matsusada Precision Inc., http://www.matsusada.com/, 2013.
[14] M. Bogdan, et al., in: Nuclear Science Symposium Conference Record, 2007. NSS '07. IEEE, volume 1, pp. 133–134.
[15] M. Bogdan, et al., in: Real Time Conference, 2009. RT '09. 16th IEEE-NPSS, pp. 443 –445.
[16] Analog Devices, http://www.analog.com/en/index.html, 2013.
[17] W. R. Leo, Techniques for Nuclear and Particle Physics Experiments, Springer-Verlag, 2 edition, 1993.
[18] T. L. Quarles, Analysis of Performance and Convergence Issues for Circuit Simulation, Ph.D. thesis, EECS Department, University of California, Berkeley, 1989.
[19] SUSUMU CO., LTD., http://www.susumu.co.jp/english/, 2013.
[20] AT90USB1287, http://www.atmel.com/devices/at90usb1287.aspx, 2013.
[21] Texas Instruments, http://www.ti.com/, 2013.
[22] J. Beringer, et al.(PDG), Physical Review D 86 (2012) 010001.

[2] The temperature dependence of the light yield is $d(LY)/dT = -1.4$ %/°C for CsI crystals[22].